



HAL
open science

Strain rate and oxidation effects on crack initiation at 600 and 650 °C in a nickel-based superalloy

Maxime Perrais, Alexandre Seror, A. Burteau, Eric Andrieu, Dominique Poquillon

► **To cite this version:**

Maxime Perrais, Alexandre Seror, A. Burteau, Eric Andrieu, Dominique Poquillon. Strain rate and oxidation effects on crack initiation at 600 and 650 °C in a nickel-based superalloy. *Materials at High Temperatures*, 2016, 33 (3), pp.241-247. 10.1080/09603409.2016.1169665 . hal-01755241

HAL Id: hal-01755241

<https://hal.science/hal-01755241>

Submitted on 30 Mar 2018

HAL is a multi-disciplinary open access archive for the deposit and dissemination of scientific research documents, whether they are published or not. The documents may come from teaching and research institutions in France or abroad, or from public or private research centers.

L'archive ouverte pluridisciplinaire **HAL**, est destinée au dépôt et à la diffusion de documents scientifiques de niveau recherche, publiés ou non, émanant des établissements d'enseignement et de recherche français ou étrangers, des laboratoires publics ou privés.



Open Archive TOULOUSE Archive Ouverte (OATAO)

OATAO is an open access repository that collects the work of Toulouse researchers and makes it freely available over the web where possible.

This is an author-deposited version published in : <http://oatao.univ-toulouse.fr/>
Eprints ID : 19781

To link to this article : DOI:10.1080/09603409.2016.1169665
URL : <http://dx.doi.org/10.1080/09603409.2016.1169665>

To cite this version : Perrais, Maxime and Seror, Alexandre and Burteau, A. and Andrieu, Eric and Poquillon, Dominique *Strain rate and oxidation effects on crack initiation at 600 and 650 °C in a nickel-based superalloy*. (2016) *Materials at High Temperatures*, vol. 33 (n° 3). pp. 241-247. ISSN 0960-3409

Any correspondence concerning this service should be sent to the repository administrator: staff-oatao@listes-diff.inp-toulouse.fr

Strain rate and oxidation effects on crack initiation at 600 and 650 °C in a nickel-based superalloy

M. Perrais^{1,2}, A. Seror², A. Burteau³, E. Andrieu¹ and D. Poquillon¹ 

Nickel-based superalloys are sensitive to an oxidation-assisted intergranular crack (OAIC) growth mechanism. Crack initiation during slow strain rate tensile tests is investigated at 600 and 650 °C, at different strain rates, with or without oxidation on a direct-aged material. A V-shaped sample geometry is used to promote damage initiation for a specific stress triaxiality. The critical mechanical loading paths inducing intergranular crack initiation as well as the effect of oxidation are discussed.

Keywords: Ni-based superalloys, Direct aged alloy 718, Oxidation, Environment assisted cracking

Introduction

Alloy 718 is a nickel-based superalloy used for a wide range of applications in fields including aerospace, chemical and nuclear engineering. Many studies have been devoted to its mechanical behaviour during fatigue tests,^{1–4} creep tests^{5–7} and creep-fatigue tests.^{8–12} However, most of them have focused on standard solution-treated and aged condition 718 alloys (STD 718) whose microstructure^{10,12} differs from the direct-aged material (DA 718). This study is devoted to DA 718 used in low-pressure turbine discs of aircraft engines. The elevated temperature fatigue crack growth behaviour in STD 718 depends on the environment, and, like many other nickel-based superalloys, is sensitive to oxidation assisted intergranular cracking (OAIC).^{7,13–16} However, fewer studies are devoted to Alloy 718 for temperatures above 450 °C but some paper showed that the alloy 718 is sensitive to intergranular cracking at 600 °C.¹⁷

Mechanical testing shows that DA 718 exhibits a higher tensile strength than STD 718.¹⁰ In the present work, crack initiation in DA 718 during slow strain rate tensile tests is investigated at 600 and 650 °C with or without oxidation. The purpose is to check the effects of strain rate (down to 10⁻⁶ s⁻¹) and oxidation on damage initiation.

The critical mechanical loading paths inducing intergranular crack initiation are determined via a dual approach: observation of crack initiation locations on V-shaped specimens (Fig. 1) and supporting finite element (FE) stress and strain calculations. To assess the role of oxidation in crack formation, tests were conducted using either a laboratory air or vacuum environment. Furthermore, some pre-oxidised samples were also tested. Mechanical tests were stopped at a different strain levels; subsequently, damage initiation sites and their corresponding occurrence frequencies were identified and recorded, thanks to detailed SEM observations.

In this article, material and experimental procedures are first detailed. Next, the results of the mechanical tests and SEM observations are presented and discussed.

Material and samples

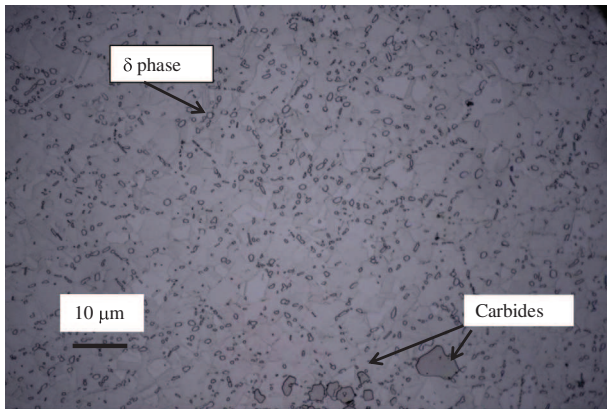
The investigated 718 alloy was obtained from a direct aged forged disc provided by SNECMA. The chemical composition of the 718 alloy is presented in Table 1. In order to get sample with the gauge length in the circumferential direction, the disc was first divided into sections. These blocks were first roughly machined to obtain trapezoid sections located in the bulk where the microstructure is homogeneous. Figure 1 shows an illustration of this microstructure characterised by roughly equiaxed small grains (6–8 µm), by globular δ phase and by the presence of occasional carbides and carbonitrides (134 per mm²). The average surface fraction of the δ precipitates is 0.5%, but the distribution is uneven due to forging. The precipitate diameter follows a log-normal distribution (an average diameter of 5.83 µm and a median diameter of 4.66 µm). Accordingly, most of the precipitates (78%) have a diameter smaller than 8 µm. Due to circular forging, carbides are often aligned in the circumferential direction. As illustrated on Fig. 1, the δ phase is localised mainly in the grain boundaries. Image analysis led to a volume fraction of globular δ phase of 3.5%. Classically, STD 718 is solution annealed after forging (1 h at 1050 °C) followed by a conventional ageing heat treatment (720 °C, 8 h, furnace cooled at 50 °C/h; 620 °C, 8 h). For DA 718, the first step is skipped. The remaining δ phase prevents grain growth during the second step and improves fatigue properties. In addition to the intragranular γ' and γ'' precipitates that are also observed in STD 718, the grain boundaries of DA 718 appear to be 'decorated' with thin δ phase precipitates where no globular δ phase precipitates are observed (Fig. 2). This nano δ platelets are 30 nm wide and can reach several hundred nanometres long. This type of precipitation is often observed but not systematic. Furthermore, a precipitate-free zone (10–15 nm width) is always observed around these thin δ phase precipitates. When 718 alloy is submitted to solution annealed heat treatment after forging, such precipitation (and PFZ) on grain boundaries is never observed. This very particular microstructure of grain boundaries in DA 718 is a key element for understanding intergranular cracks initiation. During sample preparation, particular care was taken not to change the microstructure especially in surface.

¹CIRIMAT, Université de Toulouse, CNRS, INPT, UPS, 4 allée Emile Monso – BP 44362 – 31030 TOULOUSE cedex 04, France

²SNECMA – Rond-Point René Ravaud – 77550 Moissy-Cramayel, France

³TURBOMECA – Avenue Joseph Szydlowski 64511 Bordes, France

*Corresponding author, email Dominique.Poquillon@ensiacet.fr

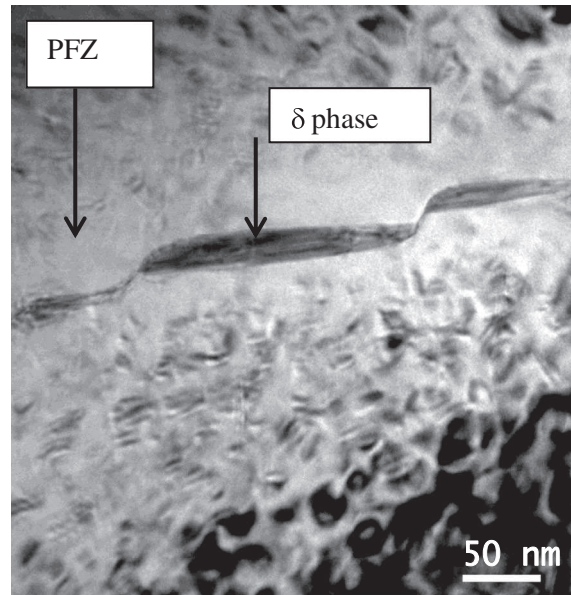


1 Typical microstructure of the alloy of this work. Optical microscopy etched using Kalling's reagent

All the specimens were machined using electrical discharge machining. Before being observed or tested, the samples were carefully polished to remove this heat-affected zone. The thickness of the HAZ due to the machining process affecting the alloy was 30 μm and was determined with SEM and TEM observations. This layer was carefully removed, thanks to successive polishing with silicon carbide papers of decreasing grit sizes (320, 400, 600 and P2400). The purpose was to obtain a mirror surface state allowing the observation of crack initiation. In order to enhance damage initiation, V-shaped specimens were used (Fig. 3). The V-shaped specimen geometry provides an area in the intrados of the V which localises strain and damage. This geometry was initially proposed by Totsuka *et al.*,^{18,19} as it enabled enhanced stressing of the sample surface and has previously been used on nickel-based alloys^{17,20} for crack initiation studies. This V-shaped sample geometry is used to promote damage initiation for a stress triaxiality (defined by the ratio of the mean stress to the equivalent stress) representative of real operating conditions. However, as stress and strain are not homogenous in such sample, tensile tests are to be coupled with finite element (FE) analysis for test design and digital image correlation (DIC) to validate. The following section will detail these two points.

Experimental procedures

FE calculations were performed to determine the scale and distribution of the local stress and strain tensor fields scale in the V-shaped specimen throughout a tensile test. These 3D calculations were performed using Zebulon finite element code²¹ together with an elastic viscoplastic isotropic constitutive law, which was identified by a standard tensile test (10^{-4}s^{-1}) and relaxation tests on the studied material. The objective of FE simulations was twofold: on the one hand, deformation in the apex of the V for an imposed displacement of the specimen grip was evaluated, and, on the other hand, the results of the simulations with the deformation fields obtained by DIC are compared. For this purpose, the photographs were taken with a Canon EOS 7D camera equipped with a macro lens and an interval timer. On the images obtained, the thickness of the V



2 TEM observation of DA 718 grain boundary with thin δ phase on the GB and a precipitate-free zone (PFZ) nearby the grain boundary

(1 mm cf. Fig. 3) was defined by 150 pixels, corresponding to 7 microns per pixel. A speckle pattern (alumina spots) was applied on the 1 mm-thick edge of the sample. This deposit was made through an aerosol sold by Mr. CHEMIE Company. The shots, thus the speckle pattern, could not be made on the faces of the V since there would be change in the surface condition, especially a risk of masking crack initiation. The images were analysed using ARAMIS software developed by GOM Company. Automatic calculations of the 2D displacements and of the plane strain tensor were achieved, thanks to this software.

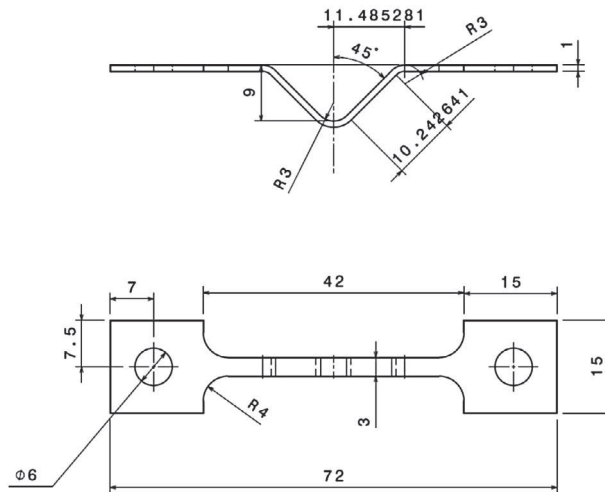
The tensile tests were carried out under air or under vacuum (10^{-5} mbar) on a screw-driven MTS testing machine at constant crosshead velocities. Three displacement rates (0.2, 2 and 20 $\mu\text{m}\cdot\text{s}^{-1}$) were used to impose three different strain rates.

The heating of the specimen was supplied by a three-zone radiative furnace. The temperature was controlled, thanks to three K type thermocouples spot-welded on the sample. Using this system, temperature gradients within the samples were maintained below 5 $^{\circ}\text{C}$. Samples were pre-heated for one hour before the test to stabilise the sample and grips temperature.

The gauge length of each tested sample was examined with a LEO 435VP SEM equipped with an EDS System (PGT IMIX). Observations focused on the intrados of the V ($4 \times 3 \text{ mm}^2$ area), which was expected to be the preferential area for damage as submitted to tension. A systematic scan of the area was conducted to locate and measure the length of the cracks. Images were made using both secondary electron and backscattered electrons to identify cracks initiated on carbides or carbonitrides. Each crack was localised and measured, and the presence of a precipitate nearby is recorded. Figure 4a illustrates a crack initiated on a carbide and propagated in the alloy, whereas Fig. 4b shows an intergranular crack initiation. Only cracks longer than 2 μm were measured. A statistical

Table 1 Chemical composition of 718 alloy (weight %)

Ni	Cr	Fe	Nb (+Ta)	Mo	Ti	Al
50–55	17–21	Bal.	4.75–5.5	2.8–3.3	0.65–1.15	0.2–0.8



3 Sketch of V-shaped specimens

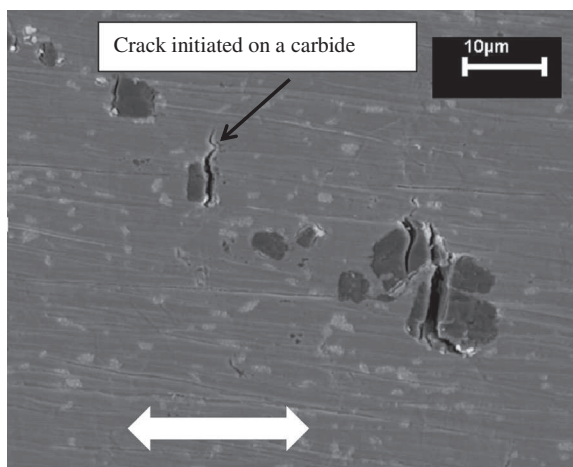
analysis of the collected data, including the number of cracks per mm^2 and the fraction of cracks linked to a carbide or a carbonitride, was also done. Tests were performed a minimum of two times for repeatability. No statistics on the depth of the cracks is available in the present study.

Results

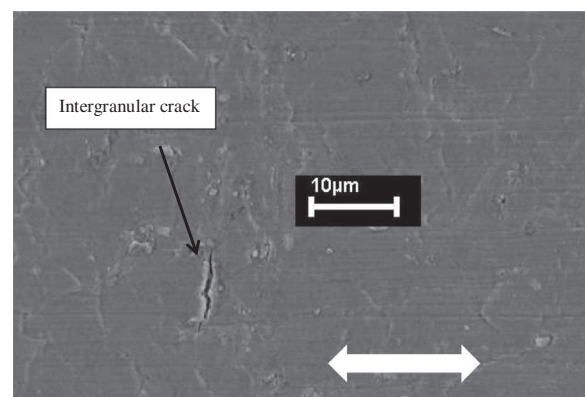
Finite element simulations

Finite element simulations have been carried out at 600 and 650 °C and all the experimental conditions have been calculated. The corresponding displacement of the specimen grip (2.5, 3.5, 4 or 5 mm) was imposed at a given displacement rate (0.2, 2 and 20 $\mu\text{m}\cdot\text{s}^{-1}$). For each simulation, we obtained the displacement vs. load curve (Fig. 5) which was compared with the experimental data, and, the strain in the apex (intrados) of the V (Fig. 6), which was compared with DIC results. Good agreement was obtained.

At 600 °C, in the range of conditions tested, the strain rate does not significantly change the force vs. displacement curve. The specimen opens out during the test and the opening of the lever arms was linked to the geometry of the sample. The maximum cumulative deformation was localised in the centre of the V, and, for the maximum elongation of 5 mm,



4a SEM observations examples of crack initiation on carbide. The tensile stress direction is indicated by the white arrow



4b SEM observations examples of intergranular crack initiation. The tensile stress direction is indicated by the white arrow

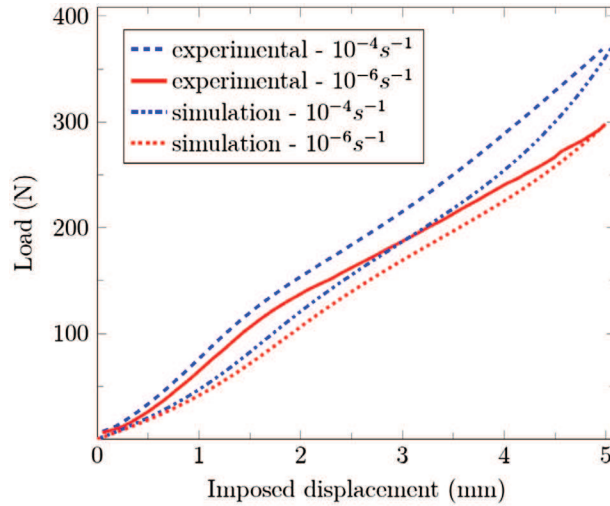
reached 7%. For imposed elongations of 2.5 mm, 3.5 mm and 4 mm, the calculated values were 2, 4 and 5.5%. The plastic zone was limited to the centre of the V (Fig. 6).

At 650 °C, strain rate effects were noticeable as illustrated on Fig. 5. As for the simulation and the experiment the displacement were imposed, for a given displacement, the strain field at 650 °C was very similar to the one at 600 °C due to the minor contribution of elasticity.

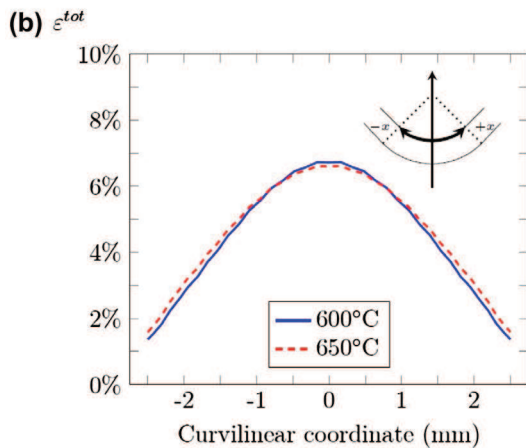
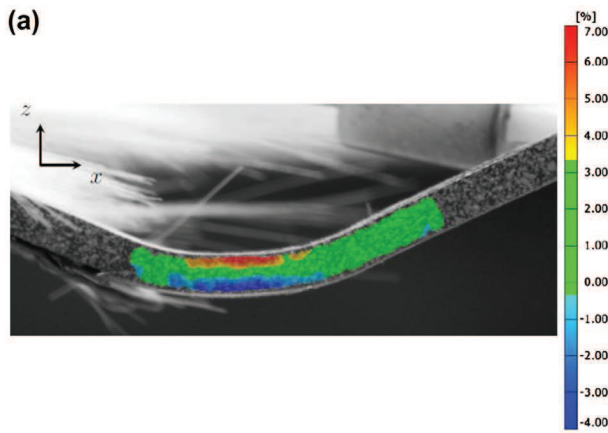
The use of a V-shaped specimen was to ensure loading of the surface material and to prevent stress redistribution, similar to a beam during a bending test, and, as a result, stress decreases in the thickness of the sample. Thanks to FE and to DIC, it was possible to calculate the strain rate in the centre of the specimen at the beginning of the test. In fact, the sample geometry and the displacement rate have been chosen using FE calculations in order to get, at the beginning of the test, the desired target strain rate in the centre on the V, on the intrados. The strain field was used to calculate the reference strain rate of the test which is the strain rate, in the tensile direction, of the point of the intrados located in the middle of the specimen. An imposed displacement rate of 0.2 $\mu\text{m}\cdot\text{s}^{-1}$ corresponded to a reference strain rate of 10^{-6} s^{-1} . Values of 10^{-5} and 10^{-4} s^{-1} corresponded to 2 and 20 $\mu\text{m}\cdot\text{s}^{-1}$.

SEM observations of crack initiations

A great number of tests (84) have been carried out under different conditions. SEM observations were used to scan



5 Comparison between experimental data and FE results for force / displacement curves obtained during the opening of the V at 650 °C. Tests carried out at in imposed displacement rate of 0.2 $\mu\text{m/s}$ (res. 20 $\mu\text{m/s}$) corresponds to a reference strain rate of 10^{-6}s^{-1} (res. 10^{-4}s^{-1})



6 Comparison between of cumulative strain fields between DIC results. (a) Experimental results at 600 °C, after 5 mm elongation at in imposed displacement rate of 0.2 $\mu\text{m/s}$. The sample thickness is 1 mm. (b) FE simulations results in the centre of the intrados of the V, at 600 and 650 °C, after 5 mm elongation at in imposed displacement rate of 0.2 $\mu\text{m/s}$

the area of interest (3x4 mm) on the intrados of the V. These characterizations revealed that the larger the imposed cumulative strain, the larger the number of crack initiations (Fig. 7). For the tests conducted for the two fastest reference strain

rates (10^{-4} and 10^{-5} s^{-1}), crack initiations were linked to a precipitates (carbides or carbonitrides). The temperature (600 or 650 °C) or the environment (air or vacuum) did not seem to change the results. When the cumulative strain exceeded 5.5%, some intergranular crack initiations were observed at the reference strain rate of 10^{-5} s^{-1} but they represented less than 20% of crack initiations.

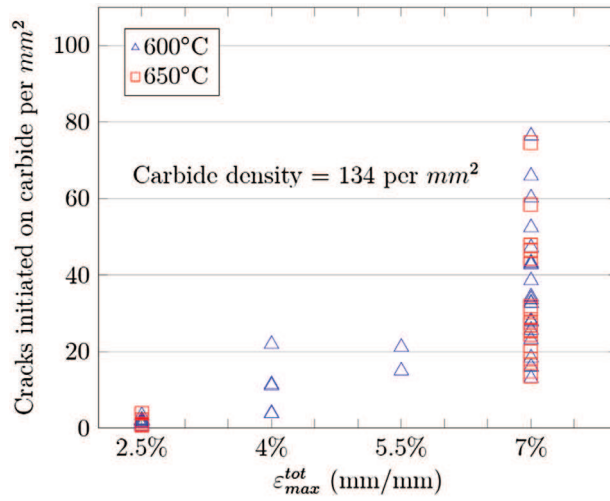
However, for the tests conducted at the slowest reference strain rate (10^{-6} s^{-1}), crack initiation was predominantly intergranular, both for vacuum and air tests (Fig. 8), and these intergranular crack initiations were located where cumulative strain was larger than 5.5% (Fig. 9). Thus, slower strain rates promoted intergranular crack initiation. Crack initiations were mostly linked to carbides for cumulative strains below 4%. Tensile tests carried out under air generated more intergranular crack at 600 °C than at 650 °C (Fig. 10). The opposite trend was observed for vacuum tests. Crack density was larger by a factor of 2 compared to results obtained under air.

In order to better understand the coupling effect due to oxidation, additional tests were performed. Some samples were pre-oxidised at 600 or 650 °C in the tensile device without loading and for the same duration (8 h) as the test duration of the longest tensile tests. After these heat treatments, SEM observations revealed no crack initiation in the matrix; however, carbide oxidation and/or fractures were noticed. Those pre-oxidised samples were then submitted to slow strain rate tensile tests at the slowest reference strain rate (10^{-6} s^{-1}) under different conditions (600/650 °C – air/vacuum).

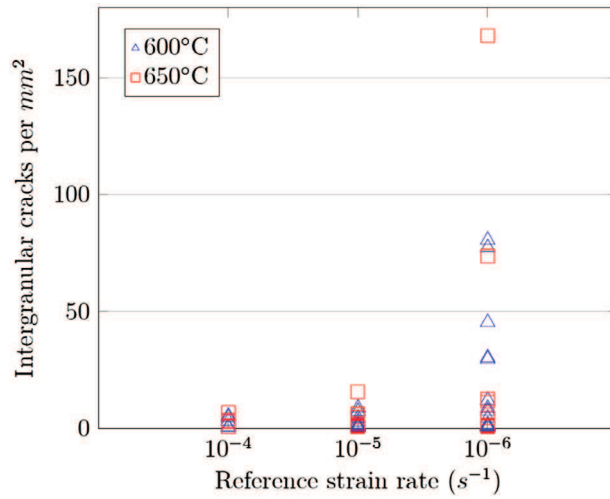
Surprisingly, intergranular crack initiation rate was lower for pre-oxidised samples (Fig. 10). And, furthermore, it decreased more for tests performed under air. The pre-oxidation seems to inhibit intergranular cracking in the DA 718 when slow strain rates tests are conducted under air. It seems that the oxidation has a beneficial effect on the intergranular crack initiation of in this alloy.

Discussion

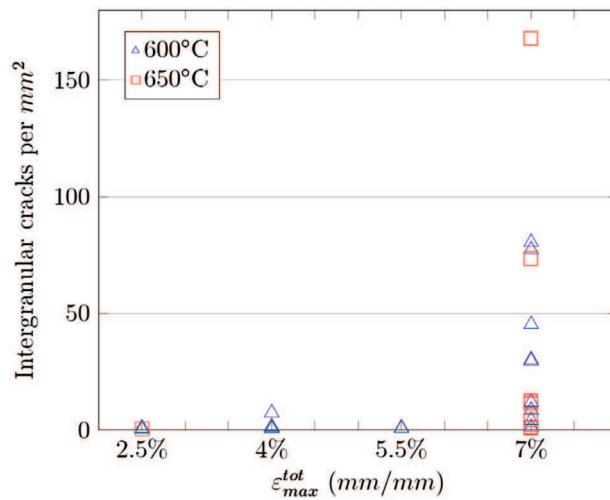
Some tensile flat specimens were tested at low strain rate to compare damages between these two geometries. For these samples, the minimum achievable strain rate was $5 \times 10^{-6} \text{ s}^{-1}$ and the gauge length was 20 times larger than the one of the V samples. However, at 600 and 650 °C no intergranular crack



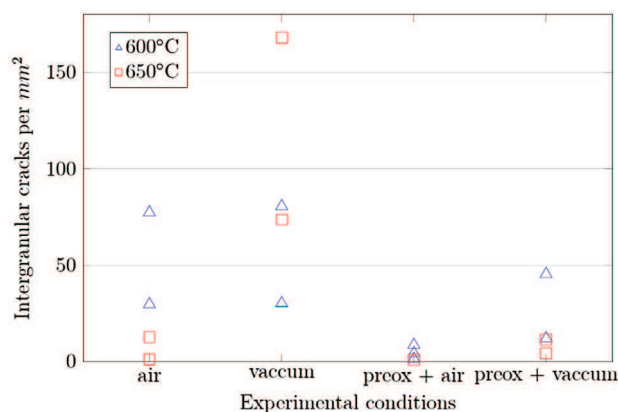
7 Diagram showing the results obtained for crack initiations on carbides or carbonitrides. Metallographic analysis of the material showed an average of 134 particles (carbides or carbonitrides) per mm^2 with very large heterogeneities



8 Diagram showing the results obtained for intergranular crack initiations as a function of the strain rate in the centre of the area where SEM observations were performed



9 Diagram showing the results obtained for intergranular crack initiations for the slowest reference strain rate ($10^{-6}s^{-1}$ corresponding to an imposed displacement rate of $0.2 \mu m/s$). Results are plotted as a function of the maximum cumulative strain in the center of the area where SEM observations were performed



10 Diagram showing the results obtained for intergranular crack initiations for a 5 mm elongation (corresponding to 7% of cumulative strain in the centre of the V), for the slowest reference strain rate (10^{-6}s^{-1} corresponding to an imposed displacement rate of $0.2\ \mu\text{m/s}$). Results are plotted as a function of experimental conditions. Tests are performed under air or vacuum, with or without 8 h of pre-oxidation at the test temperature

initiation was observed for 7% cumulative plastic strain. The main difference between the two sample geometries is the stress triaxiality, which is larger (approximately 0.5) for a V-shaped specimen instead of 0.33 for a standard tensile specimen. Furthermore, in a V-shape specimen, surface stress is promoted. Combined with specific loading conditions (plastic strain cumulated at a slow strain rate), these testing conditions appears to change the crack initiation behaviour.

Crack initiation due to carbide or carbonitride is widely reported,^{6,8,9} especially for fatigue tests on DA 718 alloys. Strain rate is a prime order parameter. Tests highlight a threshold between 10^{-5} s^{-1} and 10^{-6} s^{-1} , and the independence of environment conditions has been observed. These results could be explained by specificities of DA 718. The microstructure of the grain boundaries in DA 718 significantly differs from the one in STD 718. The presence of δ phase and of a precipitate-free zone (Fig. 2) around GB must be taken into account when one is dealing with intergranular fracture.

Some additional characterizations of the intergranular cracks were made possible, thanks to the Casting center. Some 3D crack analysis by focused ion beam (FIB) cross sectioning have been achieved. The microscope used was a FEI Helios 600i. It is a double-beam microscope combining a high-resolution SEM and a focused ion beam with gallium ions. It is also equipped with an Oxford 3D-EDS spectrometer. For the tests conducted under vacuum, oxide was never observed, neither in the cracks, nor in the grain boundaries. For the tests conducted under air, cracks were oxidised and oxygen enrichment was noticed in the grain boundary at the crack tip. The depths of all of the observed cracks were always less than $15\ \mu\text{m}$. Cross sections conducted on uncracked grain boundaries revealed no oxygen enrichment. However, as only six cracks were investigated, no statistics on the depth of the cracks are available. Observations at this scale do not allow seeing the changes in the PFZ. Only TEM characterizations at larger magnifications can reveal the changes in the microstructure and even chemical composition changes in PFZ, due to oxidation. But, unfortunately, in this study, the thin section preparation for MET has not yet been possible nearby intergranular crack.

The sensitivity to intergranular crack initiation of conventionally heat treated STD 718 can be compared with that of DA 718, as results are available in the literature^{17,20,24} for tests conducted using the same conditions. The results for DA 718 differ from those obtained for the STD 718: The effect of grain boundary precipitation on the environmental behaviour of

STD 718 appears to be an inhibition of intergranular cracking. It is known that oxidation of nickel-based superalloy induces vacancy injection in the alloy.¹⁵ These vacancies change diffusion kinetics of substitutional atoms and influence dislocation mobility^{22,23} due to coupling effects between plasticity and oxidation. Furthermore, such interactions between dislocations and solute species are known to occur during dynamic strain ageing (DSA) and Portevin Le Châtelier (PLC) regimes. For STD 718, some authors^{9,16,17,24,25} link this specific intergranular crack initiation to DSA. The grain boundaries of DA 718 are known to be weaker than those of STD 718. Local chemical composition influences plastic deformation and failure mode^{17,20} due to the role of interstitial atoms such as carbon, oxygen and nitrogen. Experimentally, it is found that if one lowers the amount of carbon interstitials, it also decreases intergranular crack initiation at $600\ ^\circ\text{C}$. In the case of DA 718, grain boundaries are embrittled by nano-delta phase precipitates and there is a great heterogeneity of mechanical behaviour between this δ phase and the matrix in the PFZ. This may contribute to stress concentration during tensile tests. According to previous studies,^{3,15} oxidation softens and changes the material microstructure nearby the surface, due to chromium depletion. Easier dislocation motion associated with vacancy injection due to oxidation may relax local stress concentrations. Therefore, these phenomena may explain why, with this specific microstructure, oxidation was found to inhibit intergranular crack initiation.

Conclusion

The objective of the present study was to investigate mechanisms for intergranular crack initiation obtained during tensile tests performed at 600 and $650\ ^\circ\text{C}$ for DA 718 and at cumulative plastic strain values below 8%. Depending on the test conditions, the failure mechanism may change drastically from crack initiation located on carbides to intergranular damage if sufficient plastic strain (more than 4%) is cumulated at a slow strain rate (10^{-6} s^{-1}). This intergranular damage development also requires specific stress conditions, as no occurrence was observed for stress triaxiality of 0.33 but was observed for 0.5. Furthermore, oxidation seems to inhibit this intergranular crack initiation. These results differ from those obtained for STD 718 under the same conditions. It is hypothesised that the role of the unique local microstructure at the grain boundary in the DA 718 may explain these results are

in accordance with discussions of micro-mechanisms found in the literature. However, further TEM investigations are required to understand changes in the microstructure or local chemical composition around grain boundaries.

Acknowledgments

The authors would like to thank Ronan Mainguy and Jean Claude Salabura for their assistance on test devices, Marie-Christine Lafont for TEM observations, Claudie Josse and Teresa Hungria (UMS Castaing) for FIB characterizations.

ORCID

D. Poquillon  <http://orcid.org/0000-0002-5006-1958>

References

1. D. Fournier and A. Pineau: 'Low cycle fatigue behavior of inconel 718 at 298 K and 823 K'. *Metall. Trans. A*, 1977, **8**, (7), 1095–1105.
2. H. H. Smith and D. J. Michel: 'Effect of environment on fatigue crack propagation behavior of alloy 718 at elevated temperatures'. *Metall. Mater. Trans. A*, 1986, **17**, (2), 370–374.
3. R. Molins, G. Hochstetter, J. C. Chassaigne and E. Andrieu: 'Oxidation effects on the fatigue crack growth behaviour of alloy 718 at high temperature'. *Acta Materialia*, 1997, **45**, (2), 663–674.
4. J. Warren and D. Y. Wei: 'The cyclic fatigue behavior of direct age 718 at 149, 315, 454 and 538°C'. *Mater. Sci. Eng. A*, 2006, **428**, (1–2), 106–115.
5. P. Shahinian and K. Sadananda: 'Crack growth behavior under creep-fatigue conditions in Alloy 718 (in nickel-chromium stainless steel)', in 'Symposium on Creep-Fatigue Interaction', 365–390, 1976, New York.
6. A. Diboine and A. Pineau: 'Creep crack initiation and growth in Inconel 718 alloy at 650 °C'. *Fatigue Fract. Eng. Mater. Struct.*, 1987, **10**, (2), 141–151.
7. M. R. Winstone, K. M. Nikbin and G. A. Webster: 'Modes of failure under creep/fatigue loading of a nickel-based superalloy'. *J. Mater. Sci.*, 1985, **20**, (7), 2471–2476.
8. J. Prybylowski and R. Ballinger: 'Influence of Microstructure on the Environmentally Assisted Cracking of Inconel 718'. *Corrosion*, 1987, **43**, (2), 111–117.
9. E. Andrieu, R. Cozar and A. Pineau: 'Effect of environment and microstructure on the high temperature behavior of alloy 718', in 'Superalloy 718 – Metallurgy and Applications', Ed. E.A. Loria, 241–256; 1989, TMS, Warrendale, PA, USA.
10. S. Deyber, F. Alexandre, J. Vaissaud and A. Pineau: 'Probabilistic life of DA 718 for aircraft engine disks', in 'Superalloy 718, 625 706 and various Derivatives', Ed. E.A. Loria, 97–110; 2005, TMS, Pittsburgh, PA, USA.
11. D. L. Prakash, M. J. Walsh, D. Maclachlan and A. M. Korsunsky: 'Crack growth micro-mechanisms in the IN718 alloy under the combined influence of fatigue, creep and oxidation'. *Int. J. Fatigue*, 2009, **31**, (11–12), 1966–1977.
12. D. D. Krueger: 'The development of direct age 718 for gas turbine aging disk application', in 'Superalloy 718 – Metallurgy and Application', Ed. E. A. Loria, 279–296; 1989, TMS, Warrendale, PA, USA.
13. E. Andrieu, H. Ghonem, A. Pineau: 'Two stage crack tip oxidation mechanism in alloy 718 S Mall', in 'Elevated temperature crack growth', Ed. T. Nicholas, 25–29; 1990, American Society of Mechanical Engineers, New York.
14. H. Ghonem and D. Zheng: 'Depth of intergranular oxygen diffusion during environment-dependent fatigue crack growth in alloy 718'. *Mater. Sci. Eng. A*, 1992, **150**, (2), 151–160.
15. E. Andrieu, R. Molins, H. Ghonem and A. Pineau: 'Intergranular crack tip oxidation mechanism in a nickel-based superalloy'. *Mater. Sci. Eng. A*, 1992, **154**, (1), 21–28.
16. L. Fournier, D. Delafosse and T. Magnin: 'Oxidation induced intergranular cracking and Portevin–Le Chatelier effect in nickel base superalloy 718'. *Mater. Sci. Eng. A*, 2001, **316**, (1–2), 166–173.
17. B. Ter-Ovanesian, D. Poquillon, J. M. Cloué and E. Andrieu: 'Influence of local mechanical loading paths on the oxidation assisted crack initiation of alloy 718'. *Mater. Sci. Eng. A*, 2012, **533**, 43–49.
18. N. Totsuka and Z. Szklarska-Smialowska: 'Effect of electrode potential on the hydrogen-induced IGSCC of alloy 600 in an aqueous solution at 350 °C'. *Corrosion*, 1987, **43**, (12), 734–738.
19. N. Totsuka, E. Lunarska, G. Cragolino and Z. Szklarska-Smialowska: 'Effect of hydrogen on the intergranular stress corrosion cracking of alloy 600 in high temperature aqueous environments'. *Corrosion*, 1987, **43**, (8), 505–514.
20. J. Deleume, D. Poquillon, V. Garat, J. M. Cloué and E. Andrieu: 'Mechanical behaviour of SSRT specimens optimized for IGSCC concerns'. *Corros. Sci.*, 2008, **50**, (3), 737–743.
21. Zebulon: <http://www.nwnumerics.com/>.
22. P. G. McCormick: 'A model for the Portevin-Le Chatelier effect in substitutional alloys'. *Acta Metallurgica*, 1972, **20**, (3), 351–354.
23. P. Wycliffe: 'Dynamic and static strain aging in substitutional and interstitial alloys', in 'TMS conference, Paper Selection, 56(CONF-840909)', 1980.
24. V. Garat, J. M. Cloué, D. Poquillon and E. Andrieu: 'Influence of Portevin–Le Chatelier effect on rupture mode of alloy 718 specimens'. *J. Nucl. Mater.*, 2008, **375**, (1), 95–101.
25. B. Max, B. Viguier, E. Andrieu and J. M. Cloué: 'A Re-examination of the Portevin-Le Chatelier Effect in Alloy 718 in Connection with Oxidation-Assisted Intergranular Cracking'. *Metall. Mater. Trans. A*, 2014, **45**, (12), 5431–5441.